AN EFFICIENT ALGORITHM FOR EM SCATTERING BY ELECTRICALLY LARGE DIELECTRIC OBJECTS USING MR-QEB ITERATIVE SCHEME AND CG-FFT METHOD

L. Zhao, T. J. Cui, and W. Li

Center for Computational Electromagnetics and the State Key
Laboratory of Millimeter Waves
Department of Radio Engineering
Southeast University
Nanjing 210096, P. R. China

Abstract—In this paper, an efficient algorithm is presented to analyze the electromagnetic scattering by electrically large-scale dielectric objects. The algorithm is based on the multi-region and quasi-edge buffer (MR-QEB) iterative scheme and the conjugate gradient (CG) method combined with the fast Fourier transform (FFT). This algorithm is done by dividing the computational domain into small sub-regions and then solving the problem in each sub-region with buffer area using the CG-FFT method. Considering the spurious edge effects, local quasi-edge buffer regions are used to suppress these unwanted effects and ensure the stability. With the aid of the CG-FFT method, the proposed algorithm is very efficient, and can solve very large-scale problems which cannot be solved using the conventional CG-FFT method in a personal computer. The accuracy and efficiency of the proposed algorithm are verified by comparing numerical results with analytical Mie-series solutions for dielectric spheres.

1. INTRODUCTION

It is of great importance to seek efficient numerical analysis of large-scale electromagnetic problems which usually require much computational time and large computer memory. The method of moments (MoM) [1] has become one of the most popular methods to compute the scattering problems in a variety of applications [2–7, 24–26]. However, MoM requires $O(N^2)$ memory usage, where N is the number of unknowns. It is not easy to satisfy the memory

requirement to solve large-scale problem using MOM even on most powerful computers. One of the approaches to overcome such a problem is the domain decomposition method, which has found wide applications in the EM community [8–12].

To reduce the computational time, the conjugate gradient (CG) method combined with the fast Fourier transform (FFT) is employed to solve the MoM matrix equation. The CG-FFT method is one of the most efficient ways to solve the volume integral equation for dielectric targets [13–21], which reduces the operation count from $O(N^2)$ to $O(N \log N)$ in each iteration.

This paper presents a hybrid technique, which combines the multi-region and quasi-edge buffer (MR-QEB) iterative scheme and the CG-FFT method, to analyze large-scale electromagnetic problems of dielectric objects. The computational domain is first divided into small sub-regions. Then the small problem in each sub-region with quasi-edge buffer region is solved using the CG-FFT method. The solutions at the processed sub-regions are used to form the problem to be solved at the next sub-regions. Once all sub-regions are analyzed, an iterative approach is used to provide the entire domain solution. The iterative technique requires solutions of fields in sub-regions a number of times until a convergence criterion is achieved. Using the proposed technique, the size of required memory can be reduced significantly. Due to the use of quasi-edge buffer regions, the field discontinuous from the spurious edge effect has been reduced, and hence the proposed algorithm has a good convergence. We have verified the accuracy and efficiency of the algorithm by comparing the numerical results with analytical results for dielectric spheres.

2. GENERAL FORMULATIONS

Consider a three-dimensional (3-D) dielectric object of arbitrary shape located in a homogeneous space which is characterized by a relative permittivities ϵ_b. Usually, the homogeneous space is free space: $\epsilon_b = 1.0$. The arbitrarily shaped dielectric object with the complex permittivity $\epsilon_r(\mathbf{r})$ is assumed to be inscribed in a cuboid $L_x \times L_y \times L_z$. Through out the paper, the time dependence of $\exp(-iwt)$ is assumed and suppressed.

Under the illumination of an incident electric field, the total electric field inside the dielectric object, $\mathbf{E}$, can be determined through the following volume integral equation

$$\mathbf{E}(\mathbf{r}) + \frac{1}{4\pi\epsilon_b} \int_V \overline{\overline{G}}(\mathbf{r}, \mathbf{r}')[\epsilon_r(\mathbf{r}') - \epsilon_b]\mathbf{E}(\mathbf{r}')d\mathbf{r}' = \mathbf{E}^{inc}(\mathbf{r}) \qquad (1)$$

where

$$\overline{\overline{G}}(\mathbf{r}, \mathbf{r}') = \frac{e^{ik_b R}}{R^5} \begin{bmatrix} G_{xx} & G_{xy} & G_{xz} \\ G_{yx} & G_{yy} & G_{yz} \\ G_{zx} & G_{zy} & G_{zz} \end{bmatrix} \tag{2}$$

is the dyadic Green's function in the homogenous space, in which the corresponding matrix elements are given by

$$G_{\xi\zeta} = (\xi - \xi')(\zeta - \zeta') \left[(k_b R)^2 + i3(k_b R) - 3 \right], \quad (\xi \neq \zeta), \tag{3}$$

$$G_{e\xi\xi} = (\xi - \xi')^2 \left[(k_b R)^2 + i3(k_b R) - 3 \right] - R^2 \left[(k_b R)^2 + i(k_b R) - 1 \right]. \tag{4}$$

Equation (1) is the integral equation for the internal electric field $\mathbf{E}$. In fact, it has an equivalent version for the induced electric current $\mathbf{J}$

$$\mathbf{J}(\mathbf{r}) + \frac{1}{4\pi} \chi(\mathbf{r}) \int_V \overline{\overline{G}}(\mathbf{r}, \mathbf{r}') \cdot \mathbf{J}(\mathbf{r}') d\mathbf{r}' = \mathbf{J}^{inc}(\mathbf{r}) \tag{5}$$

where $\chi(\mathbf{r}) = \epsilon(\mathbf{r})/\epsilon_b - 1$, and

$$\mathbf{J}(\mathbf{r}) = \chi(\mathbf{r})\mathbf{E}(\mathbf{r}), \qquad \mathbf{J}^{inc}(\mathbf{r}) = \chi(\mathbf{r})\mathbf{E}^{inc}(\mathbf{r}) \tag{6}$$

are the normalized electric current inside the dielectric object and the equivalent incident current, respectively.

We first bound the considered dielectric target in a box with the size of $L_x \times L_y \times L_z$. The box is discretized into $N_x \times N_y \times N_z$ cuboidal cells. Then the volume of each cell is $\Delta V = \Delta x \Delta y \Delta z$, where $\Delta \xi = L_\xi/N_\xi$, and N_ξ is the division number in the ξ-direction. Here and after, we let $\xi = x, y, z$. Choosing the pulse function as the basis and testing function, then Eq. (5) can be converted into a linear system of equations

$$\overline{\mathbf{Z}} \cdot \mathbf{I} = \mathbf{V} \tag{7}$$

where $\overline{\mathbf{Z}}$ is an $N \times N$ system matrix, $\mathbf{I}$ is a column vector with the coefficients of the unknown currents, and $\mathbf{V}$ is a column vector associated with the incident fields in the dielectric object. Here $N = 3N_x N_y N_z$ is the total number of unknowns. For large-scale electromagnetic problems, N is very large and it is very difficult to solve the Eq. (7) directly. To reduce the CPU time and memory requirement down to manageable levels, the MR-QEB iterative scheme is used. Splitting the computational domain into M sub-regions, the iterative scheme can be written in a form of matrix as

$$\widehat{\overline{\mathbf{Z}}}_{ii} \widehat{\mathbf{J}}_i^{(k)} = \widehat{\mathbf{W}}_i - \sum_{j \neq i, j \notin b(i)}^M \widehat{\overline{\mathbf{Z}}}_{ij} \widehat{\mathbf{I}}_j, \quad i = 1, 2, \ldots, M, \tag{8}$$

where

$$\widehat{\overline{\mathbf{Z}}}_{ii} = \left[\begin{array}{cc} \overline{\mathbf{Z}}_{ii} & \overline{\mathbf{Z}}_{ib(i)} \\ \overline{\mathbf{Z}}_{b(i)i} & \overline{\mathbf{Z}}_{b(i)b(i)} \end{array} \right], \ \widehat{\mathbf{J}}_i^{(k)} = \left[\begin{array}{c} \mathbf{I}_i^{(k)} \\ \mathbf{I}_{b(i)} \end{array} \right], \ \widehat{\mathbf{I}}_j = \left\{ \begin{array}{ll} \mathbf{I}_j^{(k)}, & j < i, \\ \mathbf{I}_j^{(k-1)}, & j > i, \end{array} \right.$$

(9)

and

$$\widehat{\overline{\mathbf{Z}}}_{ij} = \left[\begin{array}{c} \overline{\mathbf{Z}}_{ij} \\ \overline{\mathbf{Z}}_{b(i)j} \end{array} \right], \quad \widehat{\mathbf{W}}_i = \left[\begin{array}{c} \mathbf{V}_i \\ \mathbf{V}_{b(i)} \end{array} \right].$$

(10)

Here, $b(i)$ represents the appropriate buffer region, and $\mathbf{I}_j^{(k)}$ is the appropriate subvector of $\mathbf{I}$ corresponding to the jth sub-region after the kth iteration. In Eqs. (9) and (10), $\overline{\mathbf{Z}}_{ii}$ is the self-impedance matrix in the ith sub-region, $\overline{\mathbf{Z}}_{ij}$ is the multual-impedance matrix between the ith sub-region and the jth sub-region, $\overline{\mathbf{Z}}_{b(i)b(i)}$ is the self-impedance matrix in the buffer region $b(i)$, $\overline{\mathbf{Z}}_{b(i)i}$ is the multual-impedance matrix between the buffer region $b(i)$ and the ith sub-region, and $\overline{\mathbf{Z}}_{b(i)j}$ is the multual-impedance matrix between the buffer region $b(i)$ and the jth sub-region [22, 23].

To show the spirit of the MR-QEB scheme in details, a simple two-dimensional (2-D) model is described in Fig. 1. The computational domain is divided into nine sub-regions by the bold solid line. For
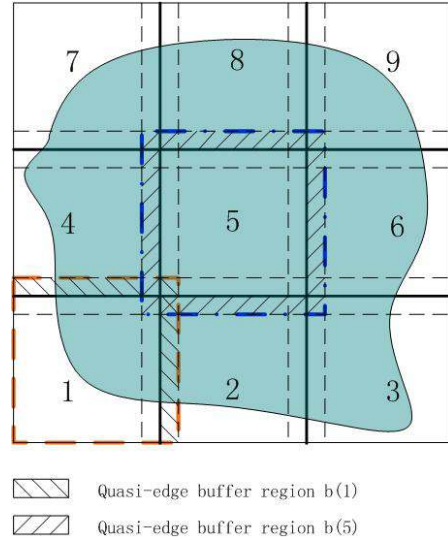

Figure 1. Subregions of a large dielectric object and the quasi-edge buffer regions.

each sub-region, the "quasi-edge buffer regions" are those areas of the scatterer immediately adjacent to the boundaries of the other sub-regions in all directions, which can be clearly seen from the 1st sub-region and 5th sub-region in Fig. 1. When the problem in a sub-region with the quasi-edge buffer regions is solved, we only store the solution in the sub-region which will be used to set up the problem to be solved at the next sub-region, and so on. Hence, there are a certain amount of redundancy in our computations, which are caused by using the quasi-edge buffer regions. However, these extra calculations include the interactions of the considered sub-region with buffer regions, which can suppress the singularities introduced by the abrupt termination of each sub-region. It is very important that the quasi-edge buffer regions needed in the proposed algorithm are very small but can dramatically enhance the stability of the iterative process.

However, the products of discrete Green's functions and electric currents in Eq. (8) are quite time and memory consuming. From the theory of Fourier transform and discrete Fourier transform (DFT) [18], the cyclic convolution of discrete signals can be fast computed using FFT. Hence, we can compute all terms in Eq. (8) rapidly by FFT. To make use of FFT, the discrete Green's functions must be extended in a larger computational domain, which can be found in [17].

After defining the extended Green's functions and the equivalent electric current, we can obtain the iterative scheme in the sth sub-region as

$$
J_{(s)\xi}(m,n,k) + \frac{1}{4\pi}\chi_{(s)}(m,n,k)\mathcal{F}^{-1}\left\{\sum_{\zeta=x,y,z}\widetilde{G}^{De}_{(ss)\xi\zeta}(i,j,l)\widetilde{J}^{De}_{(s)\zeta}(i,j,l)\right\}
$$

$$
= \chi_{(s)}(m,n,k)E^{inc}_{(s)\xi}(m,n,k)
$$

$$
- \frac{1}{4\pi}\chi_{(s)}(m,n,k)\sum_{t=1,t\neq s}^{M}\mathcal{F}^{-1}\left\{\sum_{\zeta=x,y,z}\widetilde{G}^{De}_{(st)\xi\zeta}(i,j,l)\widetilde{J}^{De}_{(t)\zeta}(i,j,l)\right\} \quad (11)
$$

where $\widetilde{G}^{De}_{(ss)\xi\zeta}(i,j,l)$ and $\widetilde{J}^{De}_{(s)\zeta}(i,j,l)$ are DFTs of $G^{De}_{(ss)\xi\zeta}(m,n,k)$ and $J^{De}_{(s)\zeta}(m,n,k)$, respectively. Similarly, the corresponding adjoint operations can also be performed using FFT. As a consequence, we can solve Eq. (11) rapidly through the CG-FFT algorithm [17]. By several iterations, we can obtain sufficiently accurate solutions.

Based on the complicity of the CG-FFT method, we can obtain the complicity in the MR-QEB-CG-FFT algorithm. Suppose that the number of total unknowns is N and the number of unknowns in a single sub-region is $N_s = N/M$ on average. The CG-FFT method reduces the computational complexities in solving the entire domain and the
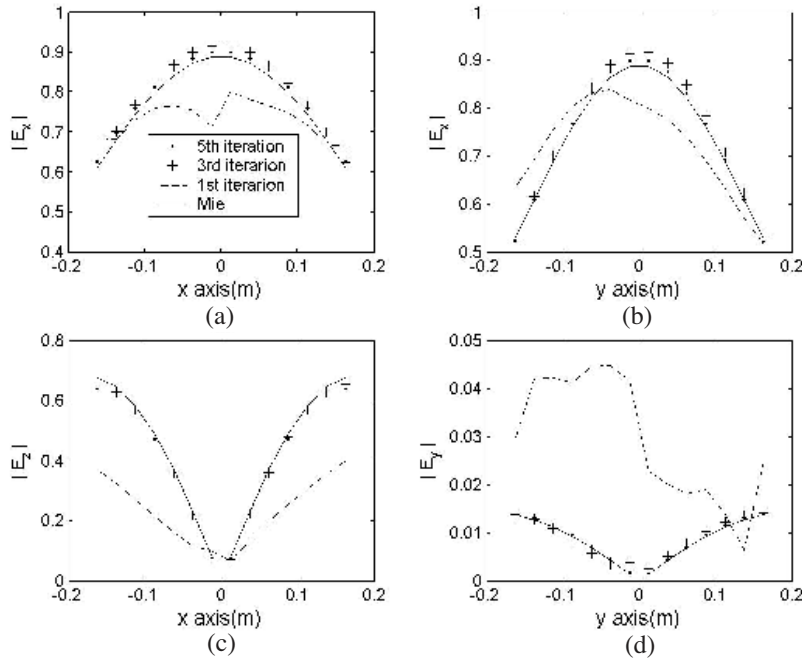
Figure 2. The distribution of internal electric field inside a dielectric sphere under the illumination of plane wave, where $\epsilon_r = 4 + i$, $f = 0.3\,\text{GHz}$, $R = 0.2\,\text{m}$, and the buffer region is 2 grids. (a) $|E_x|$ component along the central line of $y = 0$ and $z = 0$. (b) $|E_x|$ component along the central line of $x = 0$ and $z = 0$. (c) $|E_z|$ component along the central line of $y = 0$ and $z = 0$. (d) $|E_y|$ component along the central line of $x = 0$ and $z = 0$.

single sub-domain problems to $C_1 N_{it1} N \log N$ and $C_2 N_{it2} N_s \log N_s$, respectively. Here, N_{it1} and N_{it2} are iteration numbers in CG-FFT algorithms for the entire and single sub-region problems. Suppose that the number of iterations for the MR-QEB-CG-FFT algorithm is P. Then the total computational cost is estimated as

$$P \cdot M \cdot (M \cdot C_2 N_{it2} N_s \log N_s) = P \cdot M \cdot C_2 N_{it2} N (\log N - \log M). \quad (12)$$

Generally, P equals 3, C_1 and C_2 are constants used in FFT, which are nearly the same, and N_{it2} is much smaller than N_{it1}. In the process of iterations, the memory requirement in the proposed algorithm is only occupied by single sub-region. Hence the memory requirement can be drastically reduced to $O(N_s)$. This is extremely important for large-scale problems.
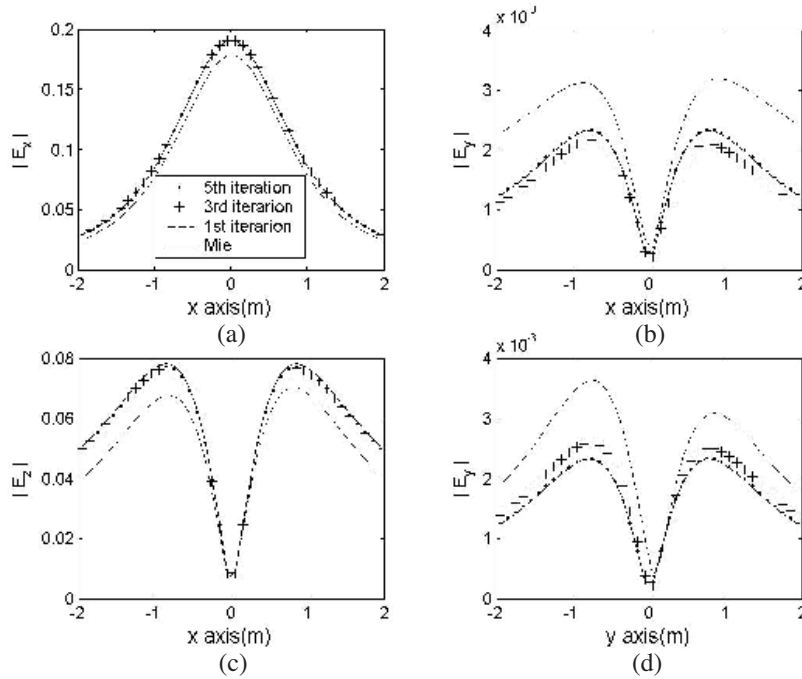
Figure 3. The distribution of scattered electric field on the observation plane $z = 1.2\,\mathrm{m}$ by the dielectric sphere under the illumination of plane wave, where $\epsilon_r = 4 + i$, $f = 0.3\,\mathrm{GHz}$, $R = 0.2\,\mathrm{m}$, and the buffer region is 2 grids. (a) $|E_x|$ component along the central line of $y = 0$. (b) $|E_y|$ component along the central line of $y = 0$. (c) $|E_z|$ component along the central line of $y = 0$. (d) $|E_y|$ component along the central line of $x = 0$.

In the MR-QEB-CG-FFT algorithm, the residual relative error on the current is used for convergence criterion, which is defined at the kth iteration as

$$error(J, k) = \frac{\| J^k - J^{k-1} \|}{\| J^k \|},\tag{13}$$

where $\| \cdot \|$ denotes the 2-norm of a column vector.

3. NUMERICAL RESULTS

To illustrate the accuracy and efficiency of the proposed MR-QEB iterative scheme combined with the CG-FFT method, we first consider the EM scattering by a sphere which is averagely split into eight
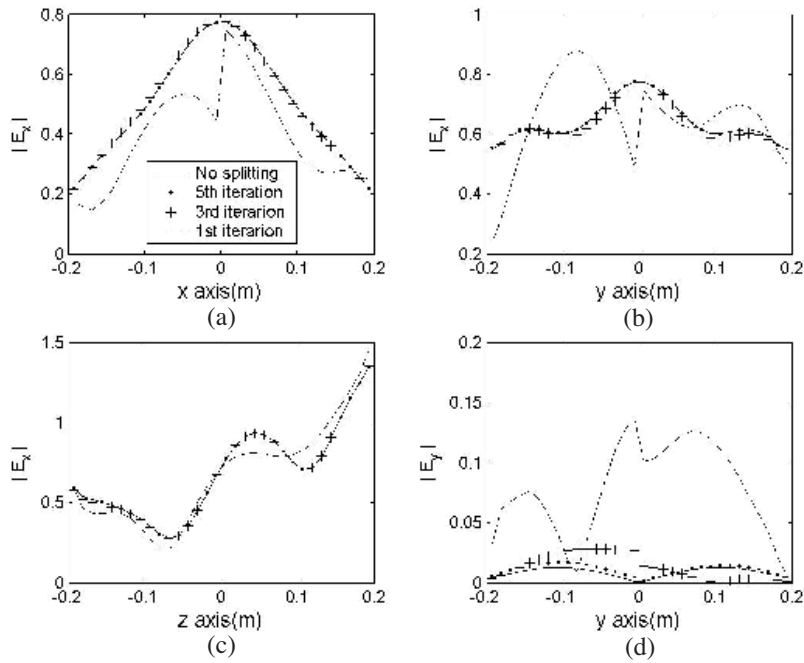
Figure 4. The distribution of internal electric field inside a dielectric cube under the illumination of plane wave, where $\epsilon_r = 4 + i$, $f = 0.6\,\text{GHz}$, $Edge = 0.4\,\text{m}$, and the buffer region is 4 grids. (a) $|E_x|$ component along the central line of $y = 0$ and $z = 0$. (b) $|E_x|$ component along the central line of $x = 0$ and $z = 0$. (c) $|E_x|$ component along the central line of $x = 0$ and $y = 0$. (d) $|E_y|$ component along the central line of $x = 0$ and $z = 0$.

sub-regions. In the following examples, the background is just free space. When the dielectric target is a sphere with $\epsilon_r = 4 + i$ and illuminated by a plane wave, the comparison of numerical results of the internal electric fields from MR-QEB-CG-FFT and analytical results is illustrated in Figs. 2 and 3, where the sphere has a radius of $0.2\,\text{m}$ and the operating frequency is $0.3\,\text{GHz}$. The incident wave is polarized in the $\hat{x}$ direction and propagating in the z direction. Here, we have used $16 \times 16 \times 16$ cubic meshes in the computational domain. From Fig. 1, we clearly observe good agreements between the numerical and analytical results in all cases after five iterations. We have also computed the scattered electric fields from the dielectric object on the observation plane $z = 1.2\,\text{m}$ and compared such results with the exact solutions,
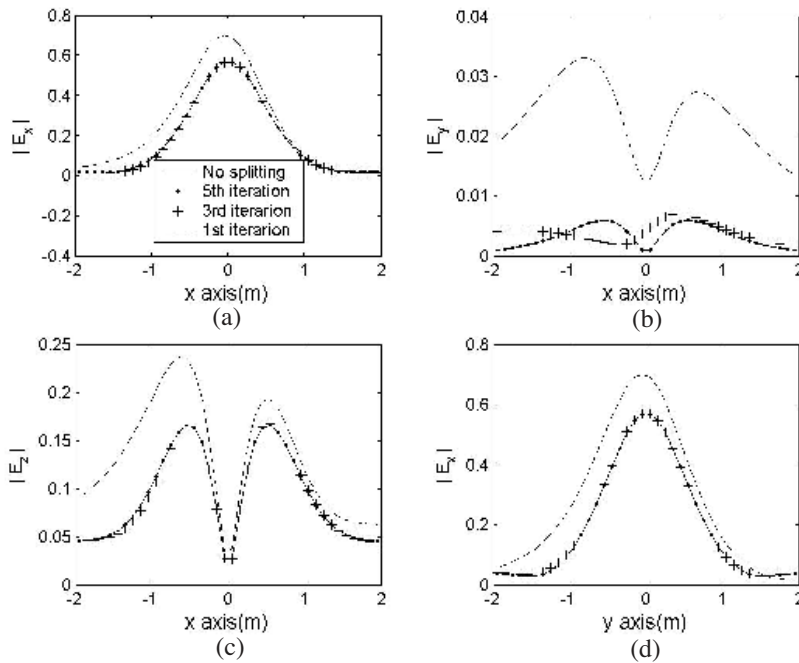
Figure 5. The distribution of scattered electric field on the observation plane $z = 1.2\,\text{m}$ by the dielectric cube under the illumination of plane wave, where $\epsilon_r = 4 + i$, $f = 0.6\,\text{GHz}$, $Edge = 0.4\,\text{m}$, and the buffer region is 4 grids. (a) $|E_x|$ component along the central line of $y = 0$. (b) $|E_y|$ component along the central line of $y = 0$. (c) $|E_z|$ component along the central line of $y = 0$. (d) $|E_x|$ component along the central line of $x = 0$.

as demonstrated in Fig. 2. Clearly, very good agreements have been observed in all field components after five iterations. From Figs. 1 and 2, we can also observe the rapid convergence behavior of the internal fields and scattered fields.

Second, we consider a dielectric cube object with $\epsilon_r = 4 + i$, which is illuminated by the same plane wave as that in Fig. 1. The cube is averagely split into four sub-regions by the plane $x = 0$ and plane $y = 0$. In such a case, the internal electric fields computed by the MR-QEB-CG-FFT algorithm are illustrated in Fig. 4, where the cube has an edge of $0.4\,\text{m}$ and the operating frequency is $0.6\,\text{GHz}$. As a comparison, numerical results of CG-FFT in the entire domain are also given in the same figure. Correspondingly, the comparison of
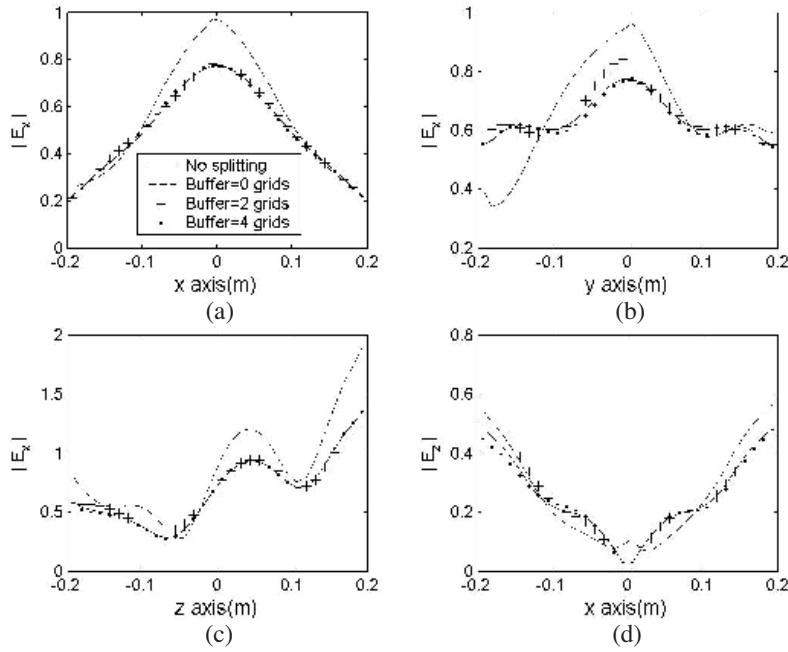
Figure 6. The distribution of internal electric field inside a dielectric cube after three iterations under the illumination of plane wave, where $\epsilon_r = 4 + i$, $f = 0.6\,\text{GHz}$, and $Edge = 0.4\,\text{m}$. (a) $|E_x|$ component along the central line of $y = 0$ and $z = 0$. (b) $|E_x|$ component along the central line of $x = 0$ and $z = 0$. (c) $|E_x|$ component along the central line of $x = 0$ and $y = 0$. (d) $|E_z|$ component along the central line of $y = 0$ and $z = 0$.
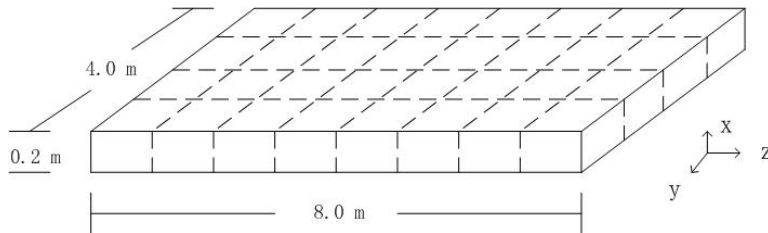

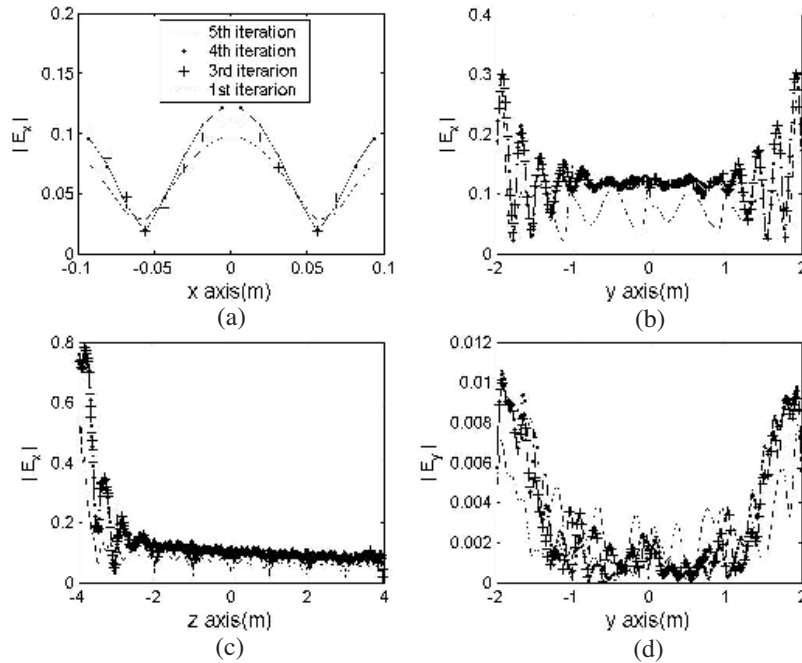**Figure 7.** A very large dielectric slab, which is divided into 32 sub-regions.

Figure 8. The distribution of internal electric field inside the dielectric slab under the illumination of plane wave, where $\epsilon_r = 4 + i0.5$, $f = 0.8\,\text{GHz}$, and the buffer region is 4 grids. (a) $|E_x|$ component along the central line of $y = 0$ and $z = 0$. (b) $|E_x|$ component along the central line of $x = 0$ and $z = 0$. (c) $|E_x|$ component along the central line of $x = 0$ and $y = 0$. (d) $|E_y|$ component along the central line of $x = 0$ and $z = 0$.

scattered electric fields on the observation plane $z = 1.2\,\text{m}$ is shown in Fig. 5. From these two figures, we obviously notice that the MR-QEB-CG-FFT solutions are rapidly convergent to the conventional CG-FFT solution after several iterations.

To see the effect of quasi-edge buffer regions, the inner field distributions after three iterations with different sizes of buffers are plotted in Fig. 6. The figure shows that the buffer region with 2–4 grids is enough to obtain stable solutions. However, the solutions are not stable if the buffer region is free. As the quasi-edge buffer regions can suppress spurious edge effects, they can improve the stability of the proposed algorithm.

After verification of the accuracy and efficiency, we apply the proposed MR-QEB-CG-FFT algorithm to study the scattering
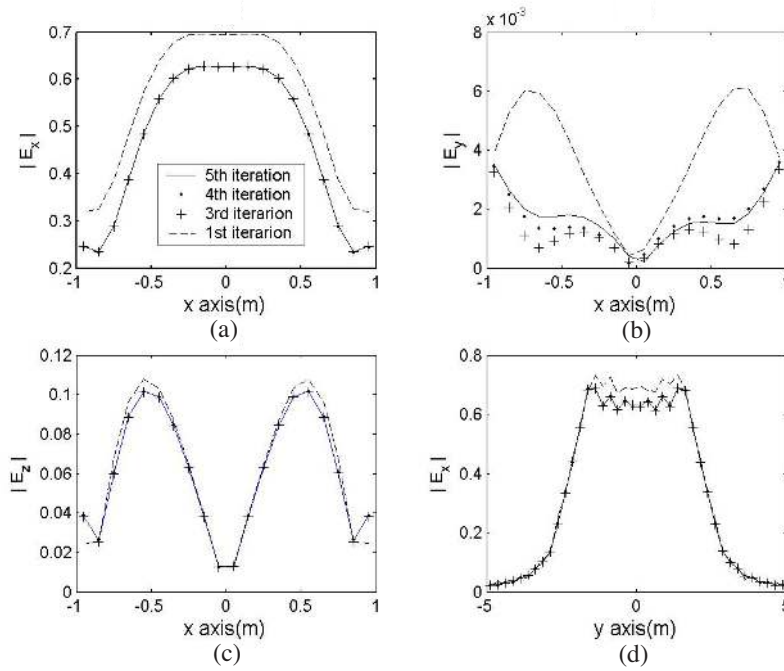
Figure 9. The distribution of scattered electric field on the observation plane $z = 5\,\mathrm{m}$ by the dielectric slab under the illumination of plane wave, where $\epsilon_r = 4 + i0.5$, $f = 0.8\,\mathrm{GHz}$, and the buffer region is 4 grids. (a) $|E_x|$ component along the central line of $y = 0$. (b) $|E_y|$ component along the central line of $y = 0$. (c) $|E_z|$ component along the central line of $y = 0$. (d) $|E_x|$ component along the central line of $x = 0$.

properties of a large dielectric slab with $\epsilon_r = 4 + i0.5$, whose dimensions and the 32 sub-domains are demonstrated in Fig. 7. Here, the computational domain is $0.2 \times 4.0 \times 8.0\,\mathrm{m}^3$, which is divided into $16 \times 320 \times 640$ cubic meshes. This is a very large problem, involving 3276800 grids and 9830400 unknowns, which cannot be solved by a personal computer with 2G memory directly even using CG-FFT method. The operating frequency is $0.8\,\mathrm{GHz}$ and the same plane wave as earlier is used as the incident wave. Figs. 8 and 9 illustrate the numerical results for the internal electric fields and the scattered fields along the observation plane $z = 5\,\mathrm{m}$ using the MR-QEB-CG-FFT algorithm. From these figures, we can clearly observe the convergence of the algorithm. The memory requirement of MR-QEB-CG-FFT is only $260\,\mathrm{MB}$. Hence, the MR-QEB-CG-FFT algorithm can economize much memory for large-scale electromagnetic problems.

4. CONCLUSIONS

In this paper, we propose a MR-QEB-CG-FFT algorithm to solve large-scale electromagnetic problems for dielectric objects. The hybrid algorithm has the ability to solve very large problems which cannot be solved in a personal computer. Good convergence have been achieved by the adoption of the quasi-edge buffer regions, which can suppress spurious edge effects. The accuracy and efficiency of the proposed algorithm has been validated using dielectric spheres, which have closed-form solutions.

ACKNOWLEDGMENT

REFERENCES

1. Harrington, R. F., *Field Computation by Moment Methods*, MacMillan, New York, 1968.
2. Goggans, P. M., A. A. Kishk, and A. W. Glisson, "Electromagnetic scattering from objects composed of multiple homogeneous regions using a region-by-region solution," *IEEE Trans. Antennas Propagat.*, Vol. 42, 865–871, 1994.
3. Graglia, R. D., P. L. E. Uslenghi, and R. S. Zich, "Moment method with isoparametric elements for three-dimensional anisotropic scatters," *Proc. IEEE*, Vol. 5, 750–760, 1989.
4. Jarem, J. M., "Method-of-moments solution of a parallel-plate waveguid aperture system," *J. Appl. Phys.*, Vol. 59, 3566–3570, 1986.
5. Livesay, D. E. and K. Chen, "Electromagnetic fields induced inside arbitrarily shaped biological bodies," *IEEE Trans. Microwave Theory Tech.*, Vol. MTT-22, 1273–1282, 1974.
6. Sarkar, T. K. and E. Arvas, "An integral equation approach to the analysis of finite microstrip antennas: Volume/surface formulation," *IEEE Trans. Antennas Propagat.*, Vol. 38, 305–312, 1990.

7. Doncker, P. D., "A potential integral equations method for electromagnetic scattering by penetrable bodies," *IEEE Trans. Antennas Propagat.*, Vol. 49, 1037–1042, 2001.

8. Smith, B., P. Bjorstad, and W. Gropp, *Domain Decomposition Parallel Multilevel Methods for Elliptic Partial Differential Equation*, Cambridge Univ. Press, New York, 1996.

9. Wohlmuth, B. I., *Discretization Methods and Iterative Solvers Based on Domain Decomposition*, Springer-Verlag, Berlin, 2001.

10. Pavarino, L. F. and A. Toselli, *Recent Developments in Domain Decomposition Methods*, Springer-Verlag, Berlin, 2002.

11. Vouvakis, M. N., Z. Cendes, and J. F. Lee, "A FEM domain decomposition mehtod for photonic and electromagentic band gap structures," *IEEE Trans. Antennas Propagat.*, Vol. 54, 721–733, 2006.

12. Sharkawy, M. A., V. Demir, and A. Z. Elsherbeni, "The iterative multi-region algorithm using a hybrid finite difference frequency domain and method of moments techniques," *Progress In Electromagnetics Research*, PIER 57, 19–32, 2006.

13. Catedra, M. F., E. Gago, and L. Nuno, "A numerical scheme to obtain the rcs of three dimension bodies of size using the conjugate gradient method and fast fourier transform," *IEEE Trans. Antennas Propagat.*, Vol. 5, 528–537, 1989.

14. Shen, C. Y., K. J. Glover, M. I. Sancer, and A. D. Varvatsis, "The discrete fourier transform method of solving differential-integral equations in scattering theory," *IEEE Trans. Antennas Propagat.*, Vol. 8, 1032–1041, 1989.

15. Zwamborn, P. and P. M. van den Berg, "The three-dimensional weak form of the conjugate gradient FFT method for solving scattering problems," *IEEE. Trans. Microwace Theory Tech.*, Vol. 9, No. 40, 1757–1766, 1992.

16. Gan, H. and W. C. Chew, "A discrete BCG-FFT algorithm for solving 3D inhomogeneous scatterer problems," *J. Electromagn. Waves Applicat.*, Vol. 9, 1339–1357, 1995.

17. Cui, T. J. and W. C. Chew, "Fast algorithm for electromagnetic scattering by buried 3D dielectric objects of large size," *IEEE Trans. Geosci. Remote Sensing*, Vol. 37, 2597–2608, 1999.

18. Weaver, J., *Applications of Discrete and Continuous Fourier Analysis*, Wiley, New York, 1983.

19. Cui, T. J., W. C. Chew, A. A. Aydiner, and Y. H. Zhang, "Fast-forward solvers for the low-frequency detection of buried dielectric objects," *IEEE Trans. Geosci. Remote Sensing*, Vol. 41, 2026–2036, 2003.

20. Millard, X. and Q. H. Liu, "A fast volume integral equation solver for electromagnetic scattering from large inhomogeneous objects in planarly layered media," *IEEE Trans. Antennas Propagat.*, Vol. 51, 2393–2401, 2003.

21. Peters, T. J. and J. L. Volakis, "Application of a conjugate gradient FFT method to scattering from thin planar material plates," *IEEE Trans. Antennas Propagat.*, Vol. 36, 518–526, 1988.

22. Brennan, C., P. Cullen, and M. Condon, "A novel iterative solution of the three dimensional electric field integral equation," *IEEE Trans. Antennas Propagat.*, Vol. 52, 2781–2784, 2004.

23. Li, W. D., W. Hong, and H. X. Zhou, "Integral equation based overlapped domain decomposition method (IE-ODDM) for the analysis of electromagnetic scattering of 3-D conduction objects," *Micro. Opt. Tech. Lett.*, Vol. 49, 265–274, 2007.

24. Wan, J. X. and C.-H. Liang, "A fast analysis of scattering from microstrip antennas over a wide band," *Progress In Electromagnetics Research*, PIER 50, 187–208, 2005.

25. Wang, S., X. Guan, D. Wang, X. Ma, and Y. Su, "Electromagnetic scattering by mixed conducting/dielectric objects using higher-order MoM," *Progress In Electromagnetics Research*, PIER 66, 51–63, 2006.

26. Li, M.-K. and W. C. Chew, "Applying divergence-free condition in solving the volume integral equation," *Progress In Electromagnetics Research*, PIER 57, 311–333, 2006.